

Modeling of Closure Phase Measurements with AMBER/VLTI - Towards Characterization of Exoplanetary Atmospheres

Viki Joergens and Andreas Quirrenbach

Sterrewacht Leiden / Leiden Observatory, PO Box 9513, NL-2300 RA Leiden, The Netherlands

ABSTRACT

Differential phase observations with a near-IR interferometer offer a way to obtain spectra of extrasolar planets. The method makes use of the wavelength dependence of the interferometer phase of the planet/star system, which depends both on the interferometer geometry and on the brightness ratio between the planet and the star. The differential phase is strongly affected by instrumental and atmospheric dispersion effects. Difficulties in calibrating these effects might prevent the application of the differential phase method to systems with a very high contrast, such as extrasolar planets. A promising alternative is the use of spectrally resolved closure phases, which are immune to many of the systematic and random errors affecting the single-baseline phases. We have modeled the response of the AMBER instrument at the VLTI to realistic models of known extrasolar planetary systems, taking into account their theoretical spectra as well as the geometry of the VLTI. We present a strategy to determine the geometry of the planetary system and the spectrum of the extrasolar planet from closure phase observations in two steps. We show that there is a close relation between the nulls in the closure phase and the nulls in the corresponding single-baseline phases: every second null of a single-baseline phase is also a null in the closure phase. In particular, the nulls in the closure phase do not depend on the spectrum but only on the geometry. Therefore the geometry of the system can be determined by measuring the nulls in the closure phase, and braking the remaining ambiguity due to the unknown system orientation by means of observations at different hour angles. Based on the known geometry, the planet spectrum can then be directly synthesized from the closure phases.

Keywords: Extrasolar planets, planetary atmospheres, closure phase, differential phase

1. INTRODUCTION

Since the first extrasolar planet candidate was discovered in 1995 orbiting the solar-like star 51 Peg (Mayor & Queloz 1995), more than 110 extrasolar planets have been detected by indirect radial velocity surveys (see e.g. Mayor et al. 2003 for recent discoveries). In order to learn more about the physics of these exoplanets and directly detect their atmospheres, observations with milliarcsecond spatial resolution and at an unprecedented dynamical range are required (e.g. 10^{-5} for 51Peg). So far, the only observational information on the spectrum of an extrasolar planet has been obtained for the transiting planet HD 209458 B (e.g. Charbonneau et al. 2002, Vidal-Madjar et al. 2004).

It has been proposed to observe extrasolar planets and their spectra with ground-based near-IR interferometry through the differential phase or closure phase method (e.g. Quirrenbach & Mariotti 1997, Akeson & Swain 1999, Quirrenbach 2000, Lopez & Petrov 2000, Segransan 2001, Vannier et al. 2004). An overview of the mathematical basis for the observations of interferometric phases of extrasolar planets has also been provided by Meisner (2004) and in particular on the web page referenced therein.

Differential phases are measured between different wavelength bands, which, in a first order approximation, are subject to the same optical pathlength fluctuations introduced by atmospheric turbulence. The resulting differential phase errors can therefore be eliminated in the data reduction. However, higher order effects due to

Further author information: (Send correspondence to V.J.)

V.J.: E-mail: viki@strw.leidenuniv.nl

random dispersion in the atmosphere as well as in the delay lines (caused mainly by variations of the humidity of the air) can be a significant source of systematic errors.

A more promising approach is the observation of closure phases, which are measured for a closed chain of three or more telescopes. The closure phase is the sum of the individual single-baseline phases of the array and is independent of atmospheric phase errors. This self-calibration technique was first recognized by Jennison (1958) and is illustrated in the following equations. The phase Φ'_{ij} measured on the baseline between telescope i and j is the true phase for this baseline Φ_{ij} plus atmospheric errors ψ_i, ψ_j introduced above the two telescopes plus some random errors ϵ_{ij} related to this baseline:

$$\begin{aligned}\Phi'_{12} &= \Phi_{12} + \psi_1 - \psi_2 + \epsilon_{12} \\ \Phi'_{23} &= \Phi_{23} + \psi_2 - \psi_3 + \epsilon_{23} \\ \Phi'_{31} &= \Phi_{31} + \psi_3 - \psi_1 + \epsilon_{31} \quad .\end{aligned}\tag{1}$$

The closure phase is the sum of the individual observed phases and it equals the sum of the true phases (plus random non-closing errors):

$$\Phi_{cl} = \Phi'_{12} + \Phi'_{23} + \Phi'_{31} = \Phi_{12} + \Phi_{23} + \Phi_{31} + (\epsilon_{12} + \epsilon_{23} + \epsilon_{31}) \quad .\tag{2}$$

Closure phase observations from the ground will be possible with the AMBER (Astronomical Multi-BEam combineR) instrument at the Very Large Telescope Interferometer (VLTI) operated by ESO. AMBER is a first-generation VLTI instrument (Petrov et al. 2003, Malbet et al. 2004) operating in the near-IR J, H, and K bands from 1.1 to 2.4 μm . It is currently undergoing commissioning at Cerro Paranal and is scheduled to be available for regular observations in 2005. With a multi-beam combiner element and a fringe dispersing mode it has the capability of combining the light of three telescopes (UTs or ATs), and performing spectrally resolved differential and closure phase observations. There are three different spectral resolutions available: low ($R = \lambda/\Delta\lambda=35$), medium ($R = 500 \dots 1000$), and high ($R = 10000 \dots 15000$).

The closure phase signal of a planetary system depends on the interferometer geometry, the hour angle of the observation, the spectra of the planet and the star, and on the planetary system geometry. We have modeled the response of the AMBER instrument at the VLTI for known extrasolar planetary systems, taking into account their theoretical spectra as well as the geometry of the VLTI. In the following, we present a method to determine the planetary system geometry and the planet spectrum from closure phase observations in two steps.

2. MODELING OF CLOSURE PHASE OBSERVATIONS OF EXOPLANETS WITH AMBER AT THE VLTI

We have written a code to calculate simulated closure phases for known extrasolar planetary systems, taking into account their theoretical spectra as well as the geometry of the VLTI. We use theoretical spectra, which have been calculated by Sudarsky, Burrows & Hubeny (2003); see their paper for the details on the underlying theory.

The complex visibility measured with a two-telescope interferometer for a planetary system with the star on axis, and under the assumption that the planet and the star are point sources, can be written as

$$V(u, v) = \frac{1 + r(\lambda)e^{-2\pi i(\Delta\alpha u + \Delta\beta v)}}{1 + r(\lambda)} \quad ,\tag{3}$$

with $r(\lambda) = I_{pl}/I_*$ being the contrast ratio between planet and star, $\vec{s} = (\Delta\alpha, \Delta\beta)$ the separation vector between star and planet in the tangent plane of the sky, and u and v the spatial frequencies, i.e., the coordinates of the projected baseline vector in units of the wavelength λ .

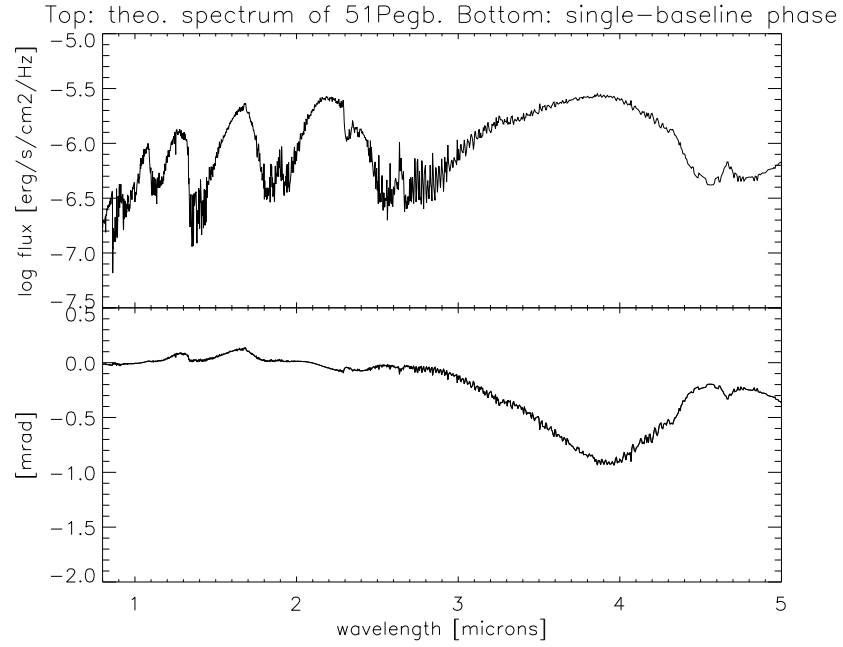


Figure 1. Spectral signal of planet in the single-baseline phase. *Top panel:* Theoretical spectrum of the giant irradiated planet orbiting the solar-like star 51 Peg (Sudarsky, Burrows & Hubeny 2003). Clearly visible are CO and H₂O absorption bands in the near-IR. *Bottom panel:* Single-baseline phases in milliradian from a calculation based on the theoretical spectrum of 51 Peg B as well as of the host star, and a simulated observation with the near-IR instrument AMBER/VLTI using the two telescopes UT1 and UT3 (baseline length 102 m). It can be clearly seen that the spectrally resolved phases contain spectral information about the planet. We note that due to atmospheric turbulence, the absolute phase is not an accessible quantity without a dual-beam facility allowing for phase referencing. For illustration, we nevertheless display them here.

The phase measured between telescopes i and j is given by the argument of (3) and can be expressed as

$$\Phi_{ij} = \arctan \left[\frac{r(\lambda) \cdot \sin(-2\pi\Delta\alpha u + \Delta\beta v)}{1 + r(\lambda) \cdot \cos(-2\pi\Delta\alpha u + \Delta\beta v)} \right] \quad (4)$$

$$= \arctan \left[\frac{r(\lambda) \cdot \sin\left(\frac{-2\pi}{\lambda} \vec{s} \cdot \vec{B}_{ij}\right)}{1 + r(\lambda) \cdot \cos\left(\frac{-2\pi}{\lambda} \vec{s} \cdot \vec{B}_{ij}\right)} \right] . \quad (5)$$

The closure phase for an array of three telescopes is calculated by summing Φ_{ij} for the three baselines:

$$\Phi_{cl} = \Phi_{12} + \Phi_{23} + \Phi_{31} . \quad (6)$$

We have retrieved the contrast ratio planet/star $r(\lambda)$ from the web site of A. Burrows. For the separation $|s|$ between star and planet the published semi-major axis is taken, but the orientation of \vec{s} is unknown, and an arbitrary value was taken for the purpose of the simulations. The projected baselines \vec{B}_{ij} are calculated for the VLTI 8 m unit telescopes (UTs).

Figures 1 and 2 show in the top panels the theoretical spectrum of the giant irradiated planet orbiting the solar-like star 51 Peg (Sudarsky, Burrows & Hubeny 2003). The most prominent features are CO and H₂O absorption bands in the near-IR. The bottom panel of Fig. 1 displays the modeled phase for the single-baseline

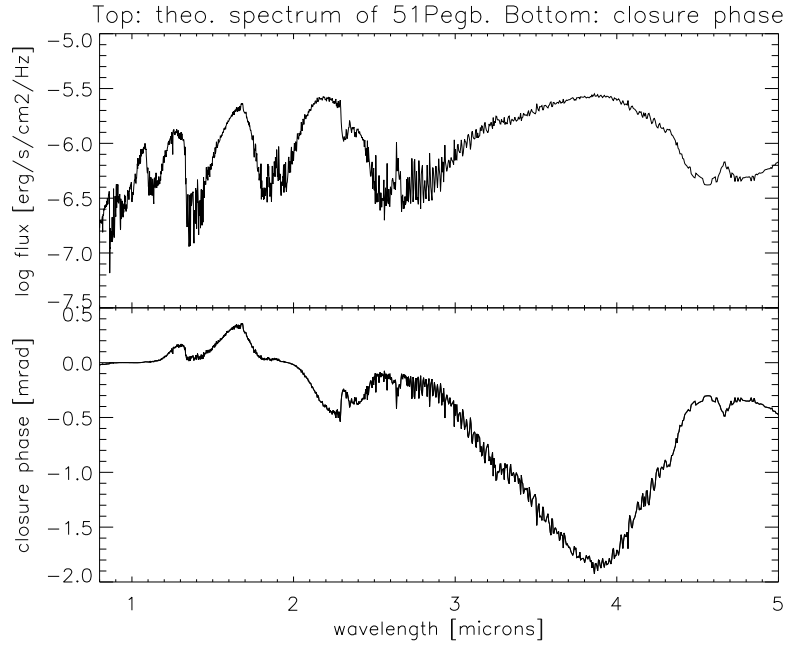


Figure 2. Spectral signal of planet in the closure phase. *Top panel:* Same as for Fig. 1. *Bottom panel:* Closure phases in milliradian calculated by us based on the theoretical spectrum of 51 Peg B as well as of the host star and a simulated observation with the near-IR instrument AMBER/VLTI using the three telescopes UT1, UT3 and UT4 (baseline lengths 102 m, 62 m, and 130 m). It is evident that the spectrally resolved closure phases contain a wealth of spectral information of the planet.

between the two telescopes UT1 and UT3 (baseline length 102 m) based on the shown theoretical spectrum of 51 Peg B as well as of the spectrum of the host star (not shown). However, due to atmospheric turbulence, the absolute phase is not an accessible quantity without a dual-beam facility allowing for phase referencing. The bottom panel of Fig. 2 shows the modeled closure phases of the 51 Peg system for the VLTI array comprised by the three telescopes UT1, UT3 and UT4 (baseline lengths 102 m, 62 m, and 130 m). It can be clearly seen that the spectrally resolved phases and closure phases contain a wealth of spectral information of the planet. Further results of the simulations are shown in Fig. 3 and Fig. 4 and are discussed later.

3. NULLS IN THE CLOSURE PHASE

In Fig. 3 we have plotted the simulated phases for two point sources with a contrast ratio of 10^{-3} and a separation of about 3 milliarcsec for the VLTI array comprised of the telescopes UT1, UT3 and UT4. For the purpose of studying the relation between the closure phase and the corresponding individual phases without the complication of the complex spectral features of the source, the contrast ratio was chosen to be constant for all wavelengths (“flat spectrum”). It can be seen from the plot that the nulls in the closure phase are always also nulls in one of the corresponding single-baseline phases. Furthermore, every second null of a single-baseline phase is also a null of the closure phase.

The condition for single-baseline phases Φ_{ij} to be zero is that the dot product between separation vector and projected baseline ($\vec{s} \cdot \vec{B}_{ij}$) equals a multiple of $\lambda/2$. The nulls in the single-baseline phase depend only on the interferometer geometry (\vec{B}_{ij}) and the planetary system geometry (\vec{s}), i.e., separation and orientation of the system, but are independent of the planet and star spectra ($r(\lambda)$).

In order to derive the condition for nulls in the closure phase, we insert the expression for Φ_{ij} (Eqn. 4) into the closure phase relation (Eqn. 6) and set the denominators to 1. The latter approximation is legitimate since

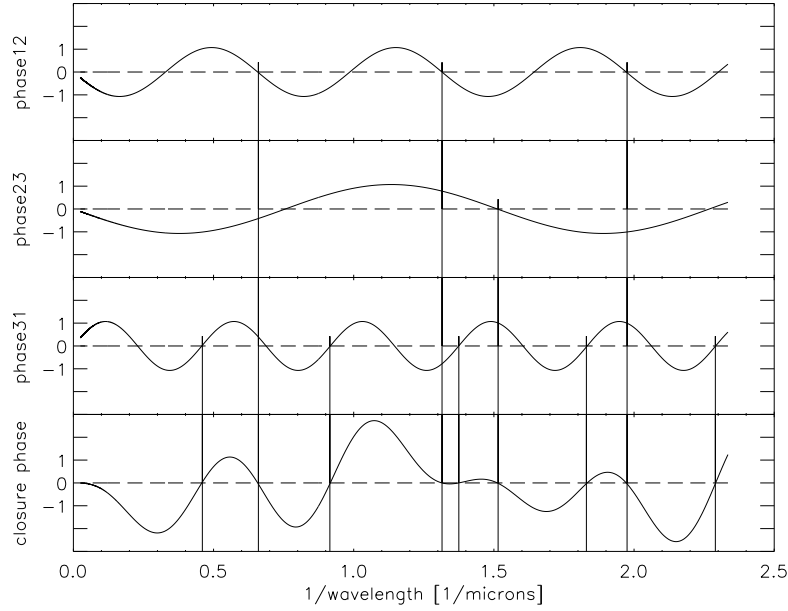


Figure 3. Relation between the closure phase and the corresponding single-baseline phases. The figure shows the simulated phase measurements for a system with a 3 milliarcsec separation at zenith observed with the VLTI telescopes UT1, UT3 and UT4 and a constant flux ratio between the two components of 10^{-3} . The three top panels display the phases measured for the three single-baselines between telescope 1 and 2, 2 and 3, and 3 and 1. (Note that they cannot be measured without a phase reference (PRIMA) and are plotted here only for theoretical considerations.) The bottom panel shows the simulated closure phase for these three telescopes. All phases are in millirad. It is obvious from this figure that the nulls in the closure phase are closely related to the nulls of the single-baselines phases: every second null of a single-baseline phase is also a null in the closure phase.

the contrast ratio between planet and star can be assumed to be much smaller than 1. (We note that this assumption is not necessary for the derivation of the conditions for the nulls in the closure phase. For simplicity we make it nevertheless.) The closure phase then becomes

$$\Phi_{cl} = \arctan \left[r \sin \left(-\frac{2\pi}{\lambda} \vec{s} \cdot \vec{B}_{12} \right) \right] + \arctan \left[r \sin \left(-\frac{2\pi}{\lambda} \vec{s} \cdot \vec{B}_{23} \right) \right] + \arctan \left[r \sin \left(-\frac{2\pi}{\lambda} \vec{s} \cdot \vec{B}_{31} \right) \right] . \quad (7)$$

Taking the closure condition that the baseline vectors add up to zero into account ($\vec{B}_{12} + \vec{B}_{23} + \vec{B}_{31} = 0$), and making the substitutions

$$\gamma := -\frac{2\pi}{\lambda} \vec{s} \cdot \vec{B}_{12} \quad (8)$$

$$p := \frac{\vec{s} \cdot \vec{B}_{31}}{\vec{s} \cdot \vec{B}_{12}} \quad (9)$$

we can rewrite Eqn. 7 as

$$\Phi_{cl} = \arctan[r \sin(\gamma)] - \arctan[r \sin(\gamma) \cos(\gamma p) + r \cos(\gamma) \sin(\gamma p)] + \arctan[r \sin(\gamma p)] . \quad (10)$$

From Eqn. 10 we can derive the conditions for nulls of the closure phase. The closure phase Φ_{cl} becomes zero if γ equals a multiple of 2π :

$$\Phi_{cl} = -\arctan[r \sin(\gamma p)] + \arctan[r \sin(\gamma p)] = 0 . \quad (11)$$

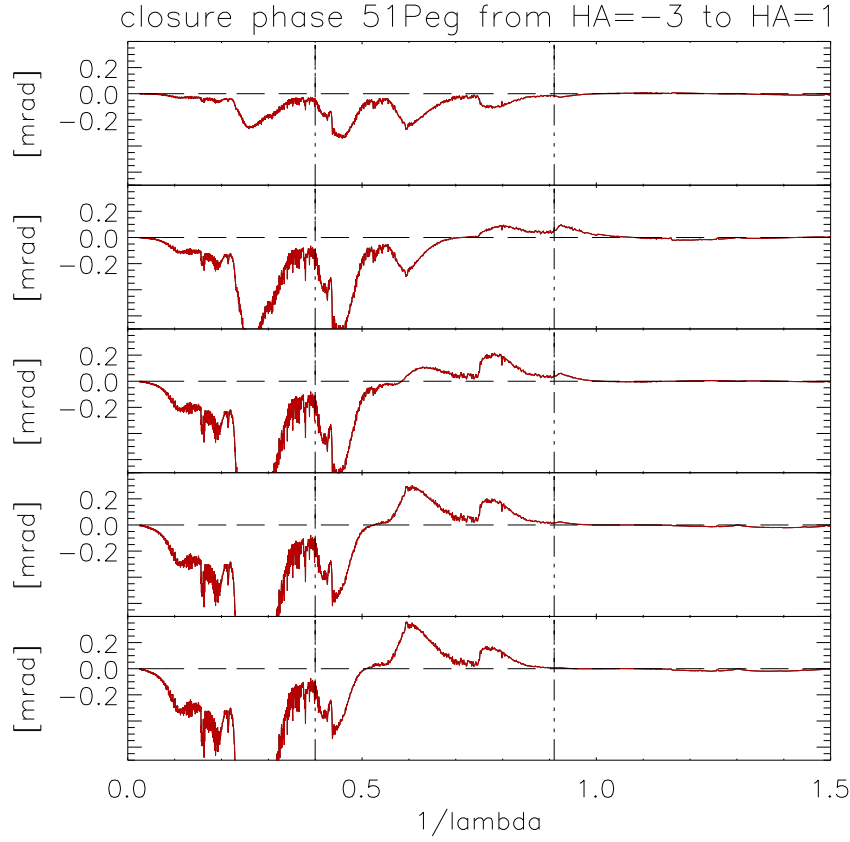


Figure 4. Closure phase time series for the planet system 51 Peg. Simulations for observations with the VLTI array UT1, UT3, UT4 for hour angles HA = -3, -2, -1, 0, +1 hr (from top to bottom). Vertical lines indicate the wavelength range covered by AMBER (the near-IR bands between 1.1 μm and 2.5 μm).

The condition $\gamma = n \cdot 2\pi$ is equivalent to $\vec{s} \cdot \vec{B}_{12} = n \cdot \lambda$. Comparing that with the condition for a null in the single-baseline phase Φ_{12} , namely $\vec{s} \cdot \vec{B}_{12} = n \cdot \lambda/2$, shows that for every second null in Φ_{12} the closure phase also has a null.

Furthermore, it can be seen from Eqn. 10 that for $\gamma \cdot p = n \cdot 2\pi$, or equivalently $\vec{s} \cdot \vec{B}_{31} = n \cdot \lambda$, the closure phase has also a null corresponding to the baseline B_{31} . A third condition for a null in Φ_{cl} exists for baseline B_{23} and it can be derived from Eqn. 10 by choosing another appropriate substitution.

To summarize, the closure phase has a null when the dot product between separation vector \vec{s} and baseline vector \vec{B}_{ij} equals multiples of λ :

$$\vec{s} \cdot \vec{B}_{ij} = n \cdot \lambda \quad \Longleftrightarrow \quad |s| \cdot |B_{ij}| \vartheta_{ij} = n \cdot \lambda \quad , \quad (12)$$

with ϑ_{ij} being the angle between \vec{s} and \vec{B}_{ij} .

This completes our proof of the relation between nulls in the closure phase and in the phases on the individual baselines illustrated in Fig. 3. It also shows that the nulls in the closure phase are independent of the planet/star contrast ratio and do only depend on the system geometry and the interferometer geometry.

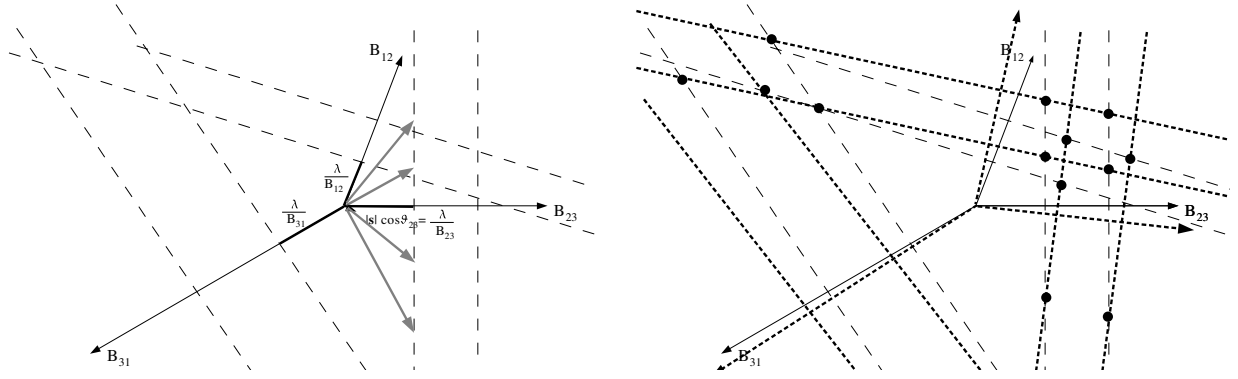


Figure 5. Possible geometries of a star – planet system as derived from nulls of the closure phase. *Left:* Determination of the nulls in the closure phase signal of a planetary system at a certain hour angle is a measure for the projection of the separation vector \vec{s} between star and planet onto one of the three projected baselines. Due to the unknown orientation ϑ_{ij} we do not know onto which one. The dashed lines indicate the possible locations of \vec{s} for the nulls corresponding to $n = 1$ and 2. *Right:* Observations at a later hour angle gives another set of lines. The possible locations for \vec{s} are now reduced to several grid points as marked by the intersections with the former lines. With a third observation, it will be possible to select the correct intersection point.

4. EARTH ROTATION SYNTHESIS

We now proceed to describe an algorithm to determine the spectrum of a planet and the geometry of the star – planet system (i.e., the angular separation and position angle of the planet with respect to the star at the time of the observation) from closure phase observations, without any a priori knowledge of these quantities. The stellar spectrum (or more precisely, the composite spectrum of the star – planet system) can be presumed to be known, however, since this is easily measurable with a simple spectrograph. Determining the planet spectrum is therefore equivalent to measuring the contrast ratio $r(\lambda)$.

As we have seen in the previous section, the nulls of the closure phase contain information about the system geometry, because they are related to the nulls of single-baseline phases. It is not known a priori, however, to which single baselines the individual nulls in the closure phase correspond. We can thus interpret Eqn. 12 as follows:

By determining a wavelength for which the closure phase is zero, we have a measure for the projection $|\vec{s}| \cdot \vartheta_{ij}$ of the separation vector \vec{s} onto one of the individual baselines \vec{B}_{ij} , but we do not know onto which one. Furthermore, we do not necessarily know the order n of the null. The geometrical locus of all possibilities for \vec{s} is therefore a set of straight lines, as shown in the left panel of Fig. 5; each line in this figure is perpendicular to one of the baselines and corresponds to an assumed set of $\{i, j, n\}$. (For clarity, only the lines corresponding to $n = 1$ and $n = 2$ are shown.)

The set of baselines vectors formed by the three telescopes changes with time due to the Earth’s rotation; a second observation therefore gives an independent constraint on the geometry as shown in the right panel of Fig. 5. The possible system geometries are now the intersections of the set of lines corresponding to the first observation with the set corresponding to the second. This discrete set of points has been marked with filled circles in the figure. A third observation will produce yet another independent set of lines. In general, this set will pass through only one of the previously marked points: this is the true separation vector.* It is thus possible

*One may be concerned that the infinite number of lines corresponding to $n = 1, 2, 3, \dots$ for each observation and each baseline may invalidate this argument. It should be noted, however, that arbitrarily high values of n can be excluded because then the nulls would be densely spaced in λ . If n is large, one would thus also observe the nulls of order $n - 1$ or $n + 1$ within the bandpass.

to derive the system geometry unambiguously with three observations.

Once the separation vector \vec{s} is known, it is straightforward to determine $r(\lambda)$ through a numerical inversion of Eqn. 10, separately for each λ . The only difficulty occurs at the nulls, where r cannot be constrained. But since three observations are needed in any case for the determination of \vec{s} , one can perform the three inversions and combine them with (wavelength-dependent) weights appropriate for their respective signal-to-noise ratios. Consider, for example, the wavelength range around $\lambda = 1.67 \mu\text{m}$ ($1/\lambda = 0.6 \mu\text{m}^{-1}$) in Fig. 4. The observation at -1 hr (third panel) gives very low signal-to-noise close to the null near $1/\lambda = 0.6 \mu\text{m}^{-1}$, but observations at other times can be used to infer the planet spectrum in this wavelength region.

5. OUTLOOK

We have shown that the separation vector and spectrum of extrasolar planets can be determined from closure phase measurements in a deterministic way, with a non-iterative algorithm, and without any a priori assumptions. For a practical application of this technique, a few additional complications will have to be considered:

- The assumption that the star and the planet are point sources will have to be relaxed. Taking into account that the star is slightly resolved by the interferometer in Eqn. 3 complicates the analysis and implies that the relation between nulls in the closure phase and the single-baseline phases is only approximately fulfilled.
- For observations from the ground, the useful wavelength range in the near-infrared is limited to the atmospheric windows and thus non-contiguous.
- The finite signal-to-noise ratio of realistic observations will lead to an uncertainty in determining the exact wavelengths of closure phase nulls. The lines and intersection points of Fig. 5 will thus be broadened.
- The non-zero time needed to accumulate sufficient signal-to-noise on the closure phase means that the interferometer geometry will change slightly during the observations. This is again equivalent to a slight broadening of the allowed regions in Fig. 5.
- If the time required to accumulate all observations is not short compared to the orbital period of the planet, the motion of the planet will also contribute an uncertainty in the derived geometry.

These practical complications will certainly be at least partially compensated by a larger number of observations; one would probably take ten or more rather than the minimum three. One could also combine the algorithm presented here with a global χ^2 minimization, in which the orbital parameters and spectrum of the planet are fitted to the observations. The purpose of our algorithm would then consist of providing a robust starting point for the χ^2 minimization algorithm, which is usually crucial to ensure convergence to the correct minimum.

The AMBER instrument has arrived on Cerro Paranal this year and the first commissioning runs have taken place. It is now necessary to determine if the necessary closure phase precision (better than 0.1 mrad, see Fig. 2) can be reached. If so, the VLTI will provide unprecedented opportunities for observations of extrasolar planets and their spectra.

ACKNOWLEDGMENTS

We are grateful to our colleagues at the Sterrewacht Jeff Meisner, Bob Tubbs and Walter Jaffe for helpful discussions on the topic of this article. VJ acknowledges support by a Marie Curie Fellowship of the European Community program “Structuring the European Research Area” under contract number FP6-501875.

REFERENCES

1. Akeson, R.L., & Swain, M.R. 1999. *Differential phase mode with the Keck Interferometer*. In *Working on the fringe: optical and IR interferometry from ground and space*. Ed. S. Unwin & R. Stachnik, Proc. ASP Conf. Vol. 194, p. 89
2. Charbonneau, D., Brown, T.M., Noyes, R.W., & Gilliland, R.L. 2002. *Detection of an Extrasolar Planet Atmosphere*, ApJ 568:377
3. Jennison, R.C. 1958. *A phase sensitive interferometer technique for the measurement of the fourier transforms of spatial brightness distributions of small angular size*, MNRAS 118:276
4. Lopez, B., & Petrov, R.G. 2000. *Direct Detection of Hot Extrasolar Planets Using Differential Interferometry*. In *From Extrasolar Planets to Cosmology: The VLT Opening Symposium*. Ed. J. Bergeron & A. Renzini, p. 565
5. Malbet, F., Driebe, T.M., Foy, R., Fraix-Burnet, D., Mathias, P., Marconi, A., Monin, J., Petrov, R.G., Stee, P., Testi, L., & Weigelt, G. 2004 *Science program of the AMBER consortium*. In *New Frontiers in Stellar Interferometry*. Ed. W.A. Traub, Proc. SPIE 5491, in press
6. Mayor, M., & Queloz, D. 1995. *A Jupiter-Mass Companion to a Solar-Type Star*, Nature 378:355
7. Mayor, M., Udry, S., Naef, D., Pepe, F., Queloz, D., Santos, N.C., & Burnet, M. 2003. *The CORALIE survey for southern extra-solar planets, XII. Orbital solutions for 16 extra-solar planets discovered with CORALIE*, A&A 415:391
8. Meisner, J. 2004. *Direct detection of exoplanets using long-baseline interferometry and visibility phase*. In *Extrasolar planets: today and tomorrow*. Ed. J.P. Beaulieu, A. Lecavelier des Etangs, & C. Terquem, ASP Conf. Ser., in press
9. Petrov, R.G., Malbet, F., Weigelt, G., Lisi, F., Puget, P., Antonelli, P., Beckmann, U., Lagarde, S., Lecoarer, E., Robbe-Dubois, S., et al. 2003. *Using the near infrared VLTI instrument AMBER*. In *Interferometry for Optical Astronomy II*. Ed. W.A. Traub, Proc. SPIE 4838, p. 924
10. Quirrenbach, A. 2000. *Astrometry with the VLT Interferometer*. In *From extrasolar planets to cosmology: the VLT opening symposium*. Ed. J. Bergeron, & A. Renzini, A., p. 462
11. Quirrenbach, A., & Mariotti, J.M. 1997. *The VLTI and the universe: conference summary*. In *Science with the VLT Interferometer*. Ed. F. Paresce, p. 339
12. Segransan, D. 2001. *The very low mass stars of the solar neighborhood: multiplicity and mass-luminosity relations*. PhD thesis, Grenoble
13. Sudarsky, D., Burrows, A., & Hubeny, I. 2003. *Theoretical spectra and atmospheres of extrasolar giant planets*, ApJ 588:1121
14. Vannier, M., Petrov, R.G., Schoeller, M., Lopez, B., Antonelli, P., Lagarde, S., Robbe-Dubois, S., Morel, S., & Rantakyro, F. 2004. *Design and tests for the correction of atmospheric and instrumental effects on color-differential phase with AMBER/VLTI*. In *New Frontiers in Stellar Interferometry*. Ed. W.A. Traub, Proc. SPIE 5491, in press
15. Vidal-Madjar, A., Désert, J.M., Lecavelier des Etangs, A., Hébrard, G., Ballester, G.E., Ehrenreich, D., Ferlet, R., McConnell, J.C., Mayor, M., & Parkinson, C.D. 2004. *Detection of oxygen and carbon in the hydrodynamically escaping atmosphere of the extrasolar planet HD 209458 b*, AJ 604:L69